

Extraordinary surface critical behavior induced by the symmetry-protected topological states of a two-dimensional quantum magnet

Zhe Wang,^{1,2} Fan Zhang,^{1,2} and Wenan Guo^{1,2,3,*}

¹*Department of Physics, Beijing Normal University, Beijing 100875, China*

²*Key Laboratory of Multiscale Spin Physics, Ministry of Education, Beijing 100875, China*

³*Beijing Computational Science Research Center, Beijing 100193, China*



(Received 27 March 2023; revised 12 June 2023; accepted 28 June 2023; published 7 July 2023)

Using quantum Monte Carlo simulations, we study spin-1/2 diagonal ladders coupled by ferromagnetic Heisenberg interactions. The model can also be viewed as usual ladders with ferromagnetic rung couplings coupled by antiferromagnetic diagonal couplings. We show that the model hosts a striped magnetic ordered phase and two topological nontrivial Haldane phases separated by two quantum critical points. We also show that the two quantum critical points are all in the three-dimensional $O(3)$ universality class irrelevant to the topological properties of the Haldane phases. The properties of the surface formed by ladder ends in the two Haldane phases are studied, showing that the surface states are both gapless due to the symmetry-protected topological bulk states. We further demonstrate that extraordinary surface critical behaviors occur at both critical points on such gapless surfaces without enhancing the surface coupling. Notably, the surface is not expected to be ordered in the three-dimensional classical $O(3)$ critical point, suggesting that the topological properties of the Haldane phases are responsible for this surface critical behavior.

DOI: [10.1103/PhysRevB.108.014409](https://doi.org/10.1103/PhysRevB.108.014409)

I. INTRODUCTION

In the Landau-Ginzburg-Wilson paradigm, phases of matter are characterized by symmetry [1]. The universality class (UC) of a critical point separating two phases is determined by the difference in symmetries on either side of the critical point and the dimensions of the system [2]. When a surface is present, the local environment near the boundary is different from that deep inside the bulk of the system; however, the divergence of correlation length at a critical point makes the influence of boundaries more pronounced; therefore, physical quantities measured on the surface also show universal behavior, which is called surface critical behavior (SCB) [3].

From the classical picture, there are ordinary, special, and extraordinary SCBs [4–6]. The singularities of an ordinary SCB is induced purely by the bulk criticality when the surface orders simultaneously with the bulk. In the case that the surface couplings are sufficiently enhanced, the surface may order in advance of the bulk when the temperature is lowered. The ordered surface exhibits extra singularities at the bulk transition point. This is called the extraordinary SCB. The special SCB is a multicritical point between the ordinary and the extraordinary transitions. For a three-dimensional (3D) model with continuous symmetry, extraordinary SCB does not apply because it is not possible to have an ordered two-dimensional (2D) surface. Recent research discovered that the surface exhibits an extraordinary-log SCB with sufficiently enhanced surface couplings at the critical point of the 3D $O(N \geq 2)$ UC [7–12]. Based on the mapping between a d -dimensional quantum system and a $(d + 1)$ -dimensional classical system,

this general picture of SCBs should apply to a quantum critical point (QCP).

However, distinct topologically ordered quantum phases that cannot be distinguished by symmetry were discovered since the study of the fractional quantum Hall effect. One class of such phases has a symmetry-protected topological (SPT) order, which cannot be mapped to a product state if only symmetric perturbations are allowed [13–15]. The symmetries of the perturbations are called the protecting symmetries. The spin-1 Haldane chain [16,17] is the first example of such a system. SPT phases are often characterized by a gap separating excitations from the ground state in bulk and the presence of gapless or degenerate edge modes. This connection between bulk and edge properties, known as bulk-edge correspondence, is caused by the topology of the state.

Now consider a critical point separating an SPT phase with a symmetry G and a phase with symmetry spontaneously broken to H in d dimensions. We may ask the following questions: Does the topological order affect the UC of the critical point, which, according to the Landau-Ginzburg-Wilson paradigm, should be determined by the difference of G and H and the dimensionality d ? Does the surface state of the SPT phase affect the SCBs associated with the critical point?

These questions have attracted recent investigations [18–20]. For the models studied previously, it was shown that the topological order does not affect the UC of the critical point. However, the gapless edge modes of the SPT phases studied previously, when merging with the bulk critical mode, lead to nonordinary SCBs at the $(2 + 1)$ -D $O(3)$ bulk critical point, which is unexpected according to the quantum-classical correspondence. Interestingly, nonordinary SCBs characterized by similar critical exponents are also found unexpectedly at the $(2 + 1)$ -D $O(3)$ quantum critical point separating

*waguo@bnu.edu.cn

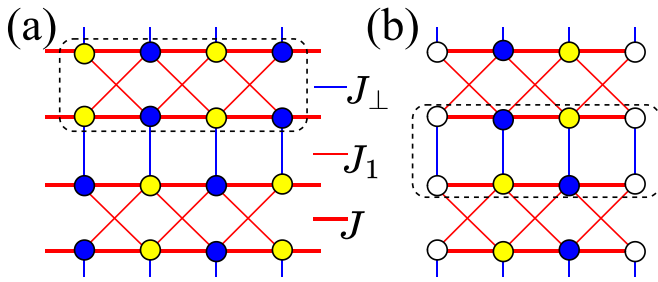


FIG. 1. The two-dimensional coupled diagonal ladders. The lattice is bipartite with sublattices A (yellow circles) and B (blue circles). (a) Periodic boundary conditions are applied in the x and y directions. A diagonal ladder is shown inside the dashed rectangular box. (b) Periodic boundary conditions are applied in the y direction, while open boundaries are applied in the x direction to expose surfaces. Open circles denote spins on the surfaces. A usual ladder is shown inside the dashed rectangular box. The interdiagonal-ladder couplings or, equivalently, the rung couplings of the usual ladders, J_{\perp} , are indicated by blue lines, interusual-ladder couplings J_1 by thin red lines, and the couplings $J > 0$ by thick red lines.

topological trivial product states and the symmetry broken phase [20–23], where the surface formed by the dangling spin chain weakly coupled to the bulk at the product state is also gapless according to the Lieb-Schultz-Mattis theorem [24]. The two nonordinary SCBs both have purely quantum but different origins.

In Ref. [20], we studied the coupled diagonal ladder (CDL) model, which is constructed by coupling the spin-1/2 diagonal ladders [25] *antiferromagnetically* (AFM) to form a

2D lattice, as illustrated in Fig. 1(a) with $J_{\perp} > 0$. In nature, there are materials described by quasi-one-dimensional spin-1 chains or spin ladders [26,27]. The diagonal ladder is the composite spin representation of a spin-1 Haldane chain, in the sense that the low-energy spectra of the two systems are identical [25]. When the ladders are weakly AFM coupled, the ground state is a 2D SPT Haldane phase (DHAF) [28]. We showed that the critical point separating the topological nontrivial phase and the Néel phase is in the (2+1)-D $O(3)$ UC, the same as that separating the topological trivial rung singlet (RS) phase and the Néel phase, shown in Fig. 2(a). At the QCP from the SPT Haldane phase to the Néel phase, we found nonordinary SCBs on the surface formed by the ends of ladders, which is attributed to the gapless edge mode of the SPT phase.

The system can also be viewed as usual two-leg ladders with AFM rung couplings J_{\perp} that are coupled by diagonal AFM bonds, as illustrated in Fig. 1(b). Both the diagonal ladder and the usual ladder with AFM rung couplings have short-ranged valence bond (VB) ground states but with different topologies, which are defined by the parity of the number of VBs crossing an arbitrary line vertical to the ladder. The ground state of the diagonal ladder is odd, with spin-1/2's localized at the ends of the ladder for open boundaries. However, that of the usual ladder with AFM rung couplings is even, with no spin-1/2's localized at the ends [25]. This explains why the RS phase does not have a gapless edge mode at the ends of the ladders, while the DHAF phase does.

A natural question arises: What are the properties of the phase that diagonal ladders are *ferromagnetically* (FM) coupled, i.e., $J_{\perp} < 0$ in Fig. 1(a); or, equivalently, what are the

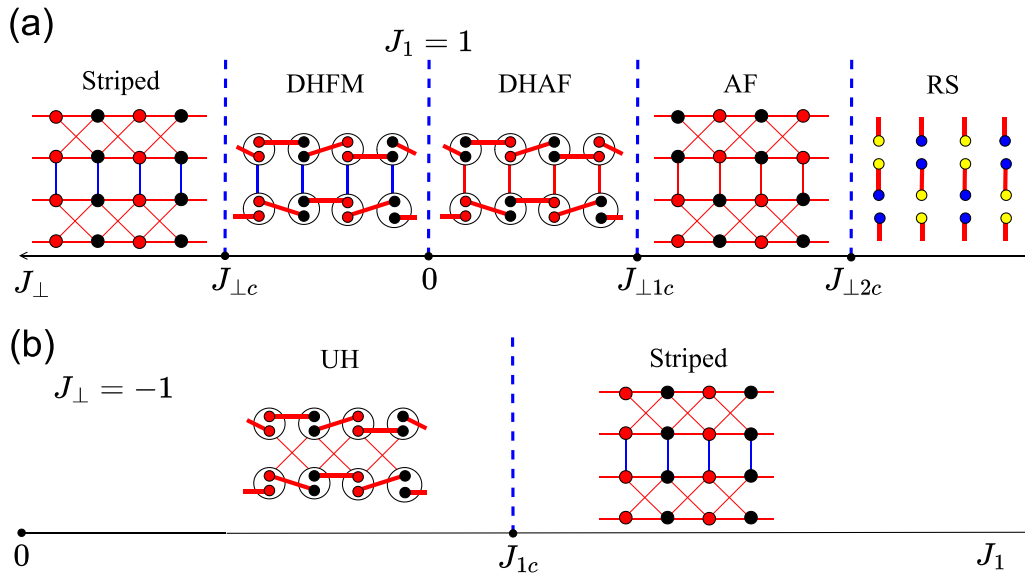


FIG. 2. Phase diagrams for (a) $J_1 = 1$ and (b) $J_{\perp} = -1$. (a) The FM-coupled diagonal-ladder Haldane phase (DHFM) and the striped magnetic order phase (striped) are separated by the QCP $J_{\perp c}$ in the region of $J_{\perp} < 0$. The AFM-coupled diagonal-ladder Haldane phase (DHAF), the antiferromagnetic phase (AFM), and the rung single phase (RS) are separated by two QCPs, $J_{\perp 1c}$ and $J_{\perp 2c}$, in the region of $J_{\perp} > 0$. (b) The usual-ladder Haldane phase (UH) and striped magnetic order phase (striped) are separated by QCP J_{1c} . A cartoon of a representative ground state is graphed in each phase. Thick-red lines denote spin singlets. The red and black solid circles represent the orientation of spins in the striped phase and AFM phase and show a particular spin configuration favored by the interladder interactions matching the typical VB state in Haldane phases. The circles in the Haldane phases indicate that two spin-1/2's form a spin-1. The $|$ and \times in the Haldane phases represent the ladder coupling.

properties of the phase that usual ladders with FM rung couplings (usual FM ladder with $J_{\perp} < 0$) are diagonally AFM coupled, as illustrated in Fig. 1(b)?

Let us start with two limits: First, the usual FM ladders are weakly AFM coupled, i.e., $0 < J_{\perp} \ll 1$. Note that the usual ladder with FM rungs behaves like a spin-1 chain and its VB ground state is odd with spin-1/2's localized at the ends of the ladder for open boundaries [25]. The ground state should be a 2D SPT Haldane phase [19,28] since the couplings between ladders are weak. The diagonal couplings can be considered effective FM couplings between neighboring spins in different ladders and thus may lead to different properties from the DHAF phase, reflected in the edge modes due to the bulk-edge correspondence. This phase is referred to as the usual ladder Haldane (UH) phase [see Fig. 2(b)]. Second, the diagonal ladders are weakly FM coupled, i.e., $|J_{\perp}| \ll 1$. Again, we expect the ground state to be a 2D SPT Haldane phase but equivalent to FM-coupled spin-1 chains. The FM coupling may lead to different properties from the DHAF phase, especially with different edge modes. We refer to this phase as the FM-coupled diagonal ladder Haldane (DHFM) phase [see Fig. 2(a)].

When the strength of the couplings between J_{\parallel} and J_{\perp} are comparable, it is natural to expect the system to transfer to a magnetically ordered striped phase. Therefore, we expect the phase diagrams sketched in Fig. 2. It is then valuable to check whether the transitions from the two SPT Haldane phases to the striped phase still obey the Landau-Ginzburg-Wilson paradigm. Suppose the two SPT Haldane phases are topologically different from the DHAF phase studied in Ref. [20]; we then ask whether the new SPTs induce different SCBs at the critical points, considering the bulk-edge correspondence.

In this paper, we answer these questions using unbiased quantum Monte Carlo (QMC) simulations [29,30]. We numerically show the presence of the magnetically ordered striped phase and the existence of two QCPs; one is between the striped phase and the SPT DHFM phase and the other is between the striped phase and the SPT UH phase. The critical exponents associated with the two QCPs are determined, showing that they all belong to the (2+1)-D O(3) UC; this fact reveals that the topological properties of the phases are irrelevant. We then show that both SPT phases have gapless edge modes on the surfaces formed by the ends of the ladders. We further demonstrate that extraordinary SCBs are realized at the two bulk critical points on the gapless surfaces without enhancing surface couplings instead of the nonordinary SCB found at the DHAF and Néel QCP in the AFM-coupled diagonal ladders. This finding shows that the SPT UH phase and the SPT DHFM phase are topologically different from the SPT DHAF phase according to the bulk-edge correspondence.

This paper is organized as follows. We describe the model and methods in Sec. II. Section III presents the results of the bulk phase transitions and surface properties of the SPT phase. We show detailed analyses of the SCBs in Sec. IV, then conclude in Sec. V.

II. MODELS AND METHODS

We study the spin-1/2 Heisenberg model on coupled diagonal ladders; see Fig. 1(a). The system can also be viewed as

coupled usual ladders, as shown in Fig. 1(b). For convenience, we write the Hamiltonian in terms of coupled diagonal ladders as follows:

$$H = \sum_{j=0} H_j + J_{\perp} \sum_{i,j=0} \mathbf{S}_{i,2j+1} \cdot \mathbf{S}_{i,2(j+1)}, \quad (1)$$

where the first sum is over the diagonal ladders with H_j describing the j th ladder written as follows:

$$H_j = J \sum_{l=0,1} \sum_i \mathbf{S}_{i,2j+l} \cdot \mathbf{S}_{i+1,2j+l} + J_{\perp} \sum_i [\mathbf{S}_{i,2j} \cdot \mathbf{S}_{i+1,2j+1} + \mathbf{S}_{i,2j+1} \cdot \mathbf{S}_{i+1,2j}], \quad (2)$$

where $l = 0, 1$ denote two legs of the j th diagonal ladder; $J > 0$ and $J_{\perp} > 0$ are intra-diagonal-ladder Heisenberg exchange interactions. The second sum describes the coupling of the neighboring ladders with the interdiagonal-ladder couplings J_{\perp} . In terms of coupled usual ladders, J and J_{\perp} are intrausual-ladder Heisenberg exchange interactions and J_{\perp} is the interusual-ladder coupling. This study is restricted to the ferromagnetic case $J_{\perp} < 0$ and set $J = 1$ to fix the energy scale.

The lattice is bipartite, and the ferromagnetic couplings J_{\perp} do not introduce magnetic frustration; therefore, the model can be studied using QMC simulations. In this paper, we use stochastic series expansion QMC simulations with the loop update algorithm [29,30] to study the bulk and SCBs of the model. Note that the allowed vertices in the case of FM and AFM bonds are different and the associated determinant loop update algorithm has to be adjusted [31]. Periodic boundary conditions applied in both the x and y lattice directions are used to study bulk phase transitions. When the surface states and SCBs are studied, periodic boundary conditions are applied along the y direction and open boundary conditions are used along the x direction to expose the surfaces, as shown in Fig. 1(b).

In our simulations, we reached linear size up to $L = 128$. The inverse temperature scales as $\beta = 2L$, considering the dynamic critical exponent $z = 1$ for the two critical points studied. Typically, 10^8 Monte Carlo samples are taken for each set of parameters.

III. BULK RESULTS

A. Symmetry-breaking phase and associated bulk phase transitions

We study several physical quantities to investigate the bulk symmetry-breaking phase and related phase transitions. In a striped magnetic phase, the spin rotational symmetry is spontaneously broken. The striped magnetization is used to describe this order as follows:

$$m_s^z(L) = \frac{1}{L^2} \sum_i (-1)^{i_x} S_i^z, \quad (3)$$

where $i_x = 1, 2, \dots, L$ is the x coordinate of the spin i . The Binder cumulant U_2 [32,33] is defined based on m_s^z as follows:

$$U_2(L) = \frac{5}{6} \left(3 - \frac{\langle m_s^z(L)^4 \rangle}{\langle m_s^z(L)^2 \rangle^2} \right), \quad (4)$$

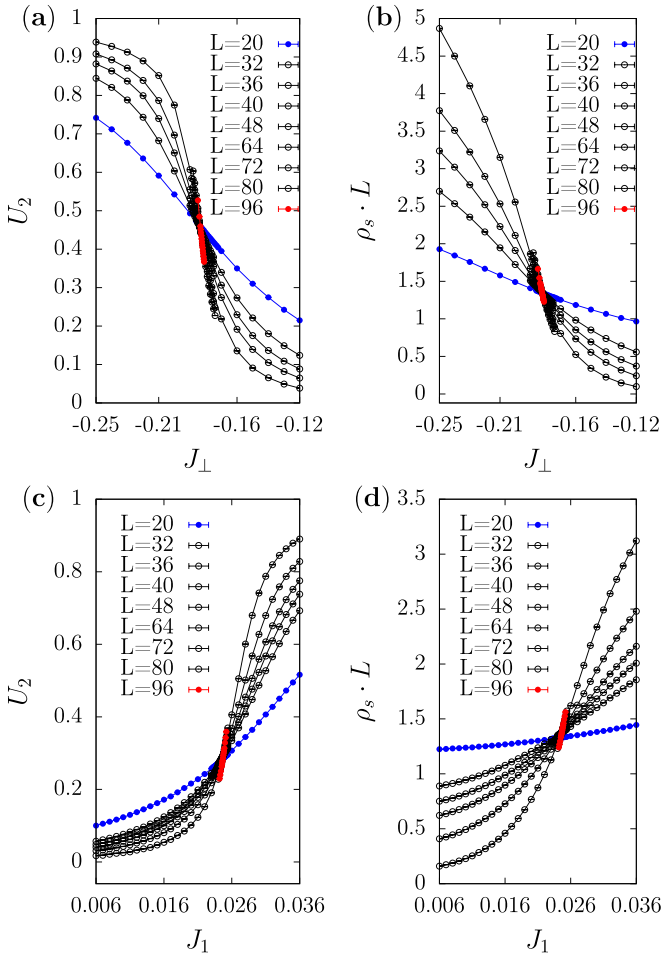


FIG. 3. Binder cumulant U_2 and spin stiffness multiplied by the system size $\rho_s L$ versus J_\perp or J_1 for different system sizes. Error bars are much smaller than the symbols. (a), (b) Results near the critical point $J_{\perp c}$ for setting $J_1 = 1$. (c), (d) Results near critical point J_{1c} for setting $J_\perp = -1$.

where $U_2(L)$ converges to 1 with increasing system size, indicating the existence of the striped magnetic order, and approaches zero with increasing system size, implying that the system is in the magnetically disordered phase. At the critical point, $U_2(L)$ is dimensionless and thus converges to a constant.

The mean spin stiffness $\rho_s(L)$ in the x and y directions is calculated through the fluctuations of the winding number of spin transport [34,35]. Similar to the Binder cumulant U_2 , ρ_s is nonzero if the state is magnetically ordered and approaches zero in the magnetically disordered state. The size dependence of $\rho_s(L)$ exactly at a QCP is expected to be as follows [36]:

$$\rho_s(L) \sim L^{2-(d+z)}, \quad (5)$$

where $z = 1$ is the dynamic exponent and $d = 2$ represents the dimensions of the model. Therefore, $\rho_s(L)L$ is expected to be dimensionless at the critical point.

We plot $\rho_s(L)L$ and $U_2(L)$ as functions of J_\perp or J_1 for different system sizes in Fig. 3. Since $U_2(L)$ and $\rho_s(L)L$ are dimensionless at a QCP, the crossings of curves for different sizes roughly indicate the transition point. Apparently, the

model is in the striped state when J_\perp is less than -0.18 for the setting $J_1 = 1$ or when J_1 is larger than 0.024 for the setting $J_\perp = -1$.

We adopt the standard $(L, 2L)$ crossing analysis for the $U_2(L)$ and $\rho_s(L)L$ curves to estimate the critical point and critical properties; see, e.g., the Supplemental Material of Ref. [37]. Let Q label U_2 or $\rho_s L$; then we define the finite-size estimator of the critical point $J_c^{(Q)}(L)$ as the crossing point of Q curves for L and $2L$, which drift toward the critical point J_c in the following way:

$$J_c^{(Q)}(L) = J_c + aL^{-1/\nu-\omega} + \dots, \quad (6)$$

where ν is the correlation length exponent, $\omega > 0$ is an effective exponent for corrections to scaling, and a is an unknown constant. At the crossing point $J_c^{(Q)}(L)$, the finite-size estimator of the exponent ν is defined as follows:

$$\frac{1}{\nu^{(Q)}(L)} = \frac{1}{\ln 2} \ln \left(\frac{s^{(Q)}(2L)}{s^{(Q)}(L)} \right), \quad (7)$$

where $s^{(Q)}(L)$ is the slope of the curve $Q(L)$ at $J_c^{(Q)}(L)$. This estimator approaches the exponent ν at speed $L^{-\omega}$ as follows:

$$\nu^{(Q)}(L) = \nu + bL^{-\omega} + \dots, \quad (8)$$

where b is an unknown constant.

The analyses based on U_2 and $\rho_s L$ yield consistent estimates of J_c and ν within the error bars. The results with higher accuracy are selected as the final results and listed in Table I. In particular, the final estimates of the two critical points are $[J_\perp = -1, J_{1c} = 0.02482(2)]$ and $[J_\perp = -0.18271(6), J_1 = 1]$.

To further determine the universal properties of the two critical points, we then calculate the static spin structure factor and the spin correlation at the longest distance in a finite system at the two estimated critical points $(J_\perp, J_1 = 1)$ and $(J_\perp = -1, J_{1c})$.

The two quantities are defined based on the spin correlation function as follows:

$$C(\mathbf{r}_{ij}) = \langle S_i^z S_j^z \rangle, \quad (9)$$

where \mathbf{r}_{ij} is the vector from site i to j . The static spin structure factor at wave vector $(\pi, 0)$ is used to describe the striped order, which is defined as follows:

$$S(\pi, 0) = \sum_{\mathbf{r}_{ij}} (-1)^{i_x - j_x} C(\mathbf{r}_{ij}), \quad (10)$$

where $i_x, j_x = 1, 2, \dots, L$ are the x coordinates of spins i and j , respectively. The spin correlation function $C(L/2, L/2)$ averages $C(\mathbf{r}_{ij})$ between two spins i and j at the longest distance $\mathbf{r}_{ij} = (L/2, L/2)$.

Using $S(\pi, 0)$ and $C(L/2, L/2)$, we extract the scaling dimension y_h of the striped magnetic field h conjugating to the striped magnetization m_s^z and the anomalous dimension η .

At a QCP, $S(\pi, 0)$ and $C(L/2, L/2)$ satisfy the following finite-size scaling forms:

$$S(\pi, 0)/L^2 \sim L^{-2(d+z-y_h)}(1 + b_1 L^{-\omega_1}) \quad (11)$$

and

$$C(L/2, L/2) \sim L^{-(d+z-2+\eta)}(1 + b_2 L^{-\omega_2}), \quad (12)$$

TABLE I. Bulk critical points and exponents. Reduced χ^2 ($R\text{-}\chi^2 = \chi^2/\text{d.o.f}$) and p value of χ^2 ($P\text{-}\chi^2$) are listed below the corresponding exponents. The universal exponents obtained by field theory (FT) and by Monte Carlo simulations (MC) on the 3D classical O(3) models are also listed for comparison.

	$J_c(U_2)$	$J_c(\rho_s L)$	$\nu(U_2)$	$\nu(\rho_s L)$	η	y_h
$J_{\perp c}$	-0.18271(6)	-0.185(3)	0.72(5)	0.70(1)	0.0350(6)	2.483(2)
R/P- χ^2	0.86/0.46	0.58/0.63	0.50/0.74	1.09/0.36	0.51/0.90	1.5/0.12
$J_{\parallel c}$	0.02482(2)	0.025(2)	0.73(4)	0.70(3)	0.035(14)	2.483(2)
R/P- χ^2	0.46/0.63	0.31/0.74	0.66/0.57	0.36/0.88	0.90/0.55	1.23/0.27
FT [38]				0.7073(35)	0.0355(25)	
MC [39]				0.7117(5)	0.0378(3)	

where $d = 2$ is the spatial dimension, $z = 1$ is the dynamical critical exponent, and ω_1 and ω_2 are the effective exponents for corrections to scaling. The two exponents y_h and η are not independent and are expected to obey the following scaling relation:

$$\eta = d + z + 2 - 2y_h. \quad (13)$$

Figure 4 shows the numerical results of $S(\pi, 0)/L^2$ and $C(L/2, L/2)$ as functions of system size L at two critical points. Fitting Eqs. (11) and (12) to the data of $S(\pi, 0)/L^2$ and $C(L/2, L/2)$, respectively, we obtain the critical exponents y_h and η at the two critical points. In these fits, we find that setting $\omega_1 = 1$ and $\omega_2 = 1$ yields good fits. The results are also presented in Table I. The two pairs of y_h and η agree well and satisfy the scaling relations Eq. (13) within the error bars.

Compared with the best-known exponents of the 3D O(3) UC [38,39], we conclude that both critical points belong to the (2+1)-D O(3) UC. Combined with the previous numerical results [20,40], these results further support that the topological order does not change the UC of the bulk phase transition, described by the Landau symmetry-breaking paradigm.

B. The Haldane phases and their surface states

We now look into the properties of the nonmagnetic phase closer.

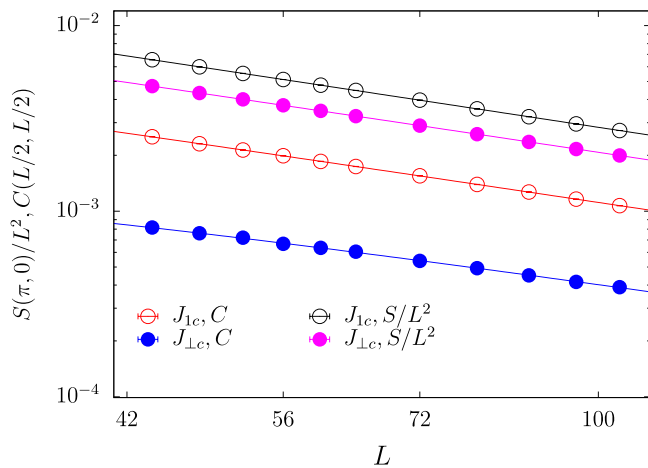


FIG. 4. $C(L/2, L/2)$ and $S(\pi, 0)/L^2$ versus system size L at the quantum critical points $(-1, J_{\parallel c})$ and $(J_{\perp c}, 1)$ on a log-log scale. Error bars are much smaller than the symbols.

An $S = 1/2$ diagonal ladder, shown inside the dashed rectangular box in Fig. 1(a), is the composite spin representation of an $S = 1$ chain [25]. Its ground state is described by the AKLT state [17], a typical configuration of which is illustrated in Fig. 2(a) at small $|J_{\perp}|$. A usual ladder with FM rung coupling $J_{\perp} < 0$, shown inside the dashed rectangular box in Fig. 1(b), also behaves like an $S = 1$ chain with a gap to excitations. Therefore, the ground state can also be represented by the AKLT state, with a typical VB configuration shown in Fig. 2(b) at small J_{\perp} . These two gapped states, corresponding to odd integer spin chains, are well-known SPT Haldane phases [16,41] with a SPT order [13,14]. With open boundaries, the ground states have two spin-1/2 spins localized at the ends of the ladder.

When the usual ladders with FM rung couplings are weakly coupled, the system is still in the SPT Haldane phase (UH) due to the gap, as illustrated in Fig. 2(b). Similarly, weakly coupled diagonal ladders stay in the SPT Haldane phase due to the gap. The antiferromagnetically coupled case (DHAF), shown in Fig. 2(a), was studied in Ref. [20]. In the current paper, we focus on the FM coupled case (DHFM), also illustrated in Fig. 2 (a).

In 1D, Haldane phases are often characterized by a hidden nonlocal order parameter, the so-called string order [25,42]. However, the string order parameter is fragile to arbitrary weak higher-dimensional couplings between such chains or ladders [14,43], which has been recently verified numerically in 2D coupled spin-1 Haldane chain (CHC) model [19] and in the 2D spin-1/2 CDLs model [20]. Nevertheless, the hallmark of the SPT phase is the presence of nontrivial surface states that are gapless or degenerate [44], which have been shown to be present in the 2D CHCs [19] and in the 2D CDLs [20]. We will show below that this is also true for the weakly FM-CDLs and weakly diagonally coupled usual ladders with FM rung couplings.

To study the surface states on the surfaces perpendicular to the ladders [see Fig. 1 (b)], we calculate the surface parallel correlation $C_{\parallel}(L/2)$, which averages $C(\mathbf{r}_{ij})$ between two surface spins i and j at the longest distance $L/2$.

Figure 5 shows $C_{\parallel}(L/2)$ at $(J_{\perp} = -1, J_{\parallel} = 0.016)$ sitting in the UH phase and $(J_{\perp} = -0.08, J_{\parallel} = 1)$ sitting in the DHFM phase. In both cases, we see that $C_{\parallel}(L/2)$ decays with system size L in a power law as follows:

$$C_{\parallel}(L/2) \sim L^{-p}. \quad (14)$$

We find $p = 2.6(1)$ for the former case and $p = 0.62(2)$ for the latter case, meaning that both surface states are gapless.

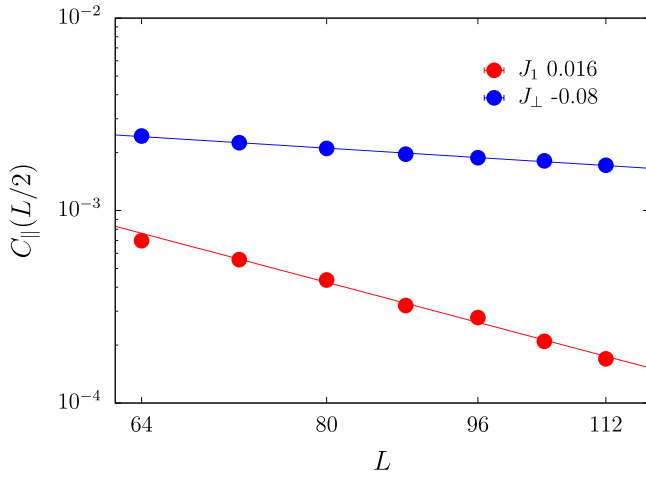


FIG. 5. Surface correlation $C_{\parallel}(L/2)$ versus system size L on a log-log scale. $C_{\parallel}(L/2)$ are calculated at ($J_{\perp} = -0.08, J_{\parallel} = 1$) in the DHFM phase and ($J_{\perp} = -1, J_{\parallel} = 0.016$) in the UH phase. Algebraically decaying with L is observed for both cases, showing two gapless surface states.

Similar power-law decay occurs on the surface of the DHAF phase [20]. Notably, the surface configurations are different there, as mentioned in the Introduction. In the DHFM phase, the interladder couplings are ferromagnetic $J_{\perp} < 0$ instead of AFM in the DHAF phase, while in the UH phase, the ladders are coupled by diagonal AFM couplings, inducing effective FM couplings between two neighboring spins in two ladders. The vanishing in power law of the parallel surface correlation demonstrates the naive idea of thinking of the surface as a ferromagnetic chain of $S = 1/2$ spins localized at the ends of the ladders, which is ordered, is incorrect. The gapless surface states purely reflect the topological order of the bulk.

IV. SURFACE CRITICAL BEHAVIORS

In this section, we study the SCBs at the two bulk critical points at ($J_{\perp} = -1, J_{\parallel c}$) and ($J_{\perp c}, J_{\parallel} = 1$).

In addition to the surface correlation $C_{\parallel}(L/2)$, we calculate another spin correlation $C_{\perp}(L/2)$ and the squared ferromagnetic surface magnetization $m_1^2(L)$, where $C_{\perp}(L/2)$ averages $C(\mathbf{r}_{ij})$ between spin i fixed on the surface and spin j located at the center of the bulk, with \mathbf{r}_{ij} perpendicular to the surface and $|j - i| = L/2$. The surface magnetization $m_1(L)$ is defined as follows:

$$m_1(L) = \frac{1}{L} \sum_{i \in \text{surface}} S_i^z, \quad (15)$$

where the summation is restricted for spins on the surface.

At a bulk critical point, for ordinary, special, and extraordinary SCBs, the finite-size scaling behavior of the two correlations is characterized by two anomalous dimensions η_{\parallel} and η_{\perp} , respectively [4], as follows:

$$C_{\parallel}(L/2) = C_{\parallel} + a_1 L^{-(d+z-2+\eta_{\parallel})} + a_2 L^{-1} + \dots \quad (16)$$

and

$$C_{\perp}(L/2) = b_1 L^{-(d+z-2+\eta_{\perp})} + b_2 L^{-1} + \dots, \quad (17)$$

where a_i and b_i are unknown constants, the $1/L$ terms are the leading correction to scaling due to analytic contributions, $C_{\parallel} = 0$ in ordinary or special SCBs, and $C_{\parallel} \neq 0$ characterizes the long-range order on the surface in an extraordinary SCB. The squared surface magnetization follows the scaling form [4]

$$m_1^2(L) = m_1^2 + c_1 L^{-2(d+z-1-y_{h1})} + c_2 L^{-1} + \dots, \quad (18)$$

where y_{h1} is the scaling dimension of the surface field h_1 ; $1/L$ is the leading contribution from analytic terms; c_i are unknown constants; and m_1^2 should be equal to C_{\parallel} , corresponding to the squared magnetization on the surface in an extraordinary SCB. For our model, $d = 2$ and $z = 1$.

The three exponents y_{h1} , η_{\parallel} , and η_{\perp} are different for ordinary, special, and extraordinary transitions; however, they are related through the following scaling relations [45]:

$$2\eta_{\perp} = \eta_{\parallel} + \eta \quad (19)$$

and

$$\eta_{\parallel} = d + z - 2y_{h1}, \quad (20)$$

where η is the anomalous magnetic scaling dimension of the bulk critical point in the $d + z$ spacetime. We use these physical quantities in the remainder of this section to examine SCBs. Two extraordinary SCBs at different bulk critical points are found.

For the 3D model with a continuous symmetry-breaking critical point, classical theory does not support extraordinary SCB because its 2D surface cannot be ordered; hence, no special SCB is available. However, when quantum mechanics sets in, it is possible that the (1+1)-D surface becomes long-range ordered due to coupling to a (2+1)-D O(3) QCP [46] and exhibits extraordinary SCBs. Numerical results have found such extraordinary SCBs in different models [21,23].

A novel extraordinary-log SCB was proposed for a surface critical state at a 3D O(N) critical point by Metlitski [7] for $2 \leq N < N_c$, in which the spin correlation decays logarithmically, as follows:

$$C_{\parallel}(L) \propto \log(L/L_0)^{-q}, \quad (21)$$

where L_0 is a nonuniversal constant. The surface magnetization $m_1^2(L)$ also decays logarithmically with the same exponent q . This extraordinary-log SCB has been verified numerically in the classical 3D O(3) model [8] and 3D O(2) model [9]. This behavior was also found on the dangling-chain surface in the spin-1 dimerized Heisenberg model [47], suggesting that such SCB may apply to 2D QCP for the integer spin model.

Previous studies [19,20] on QCPs between SPT phases and O(3) symmetry-breaking phases in (2+1)-D have found that the gapless edge modes of the SPT phases lead to nonordinary SCBs that are unexpected according to the quantum-classical correspondence. Such nonordinary SCBs show no surface order and have different exponents from the ordinary SCB of the 3D O(3) UC. The exponents are similar to the exponents of the SCBs found at the (2+1)-D O(3) QCPs separating the topological trivial product states and the symmetry-breaking phase [20–23], where the surface is a dangling $S = 1/2$ chain at the product state and thus is also gapless, according to the Lieb-Schultz-Mattis theorem.

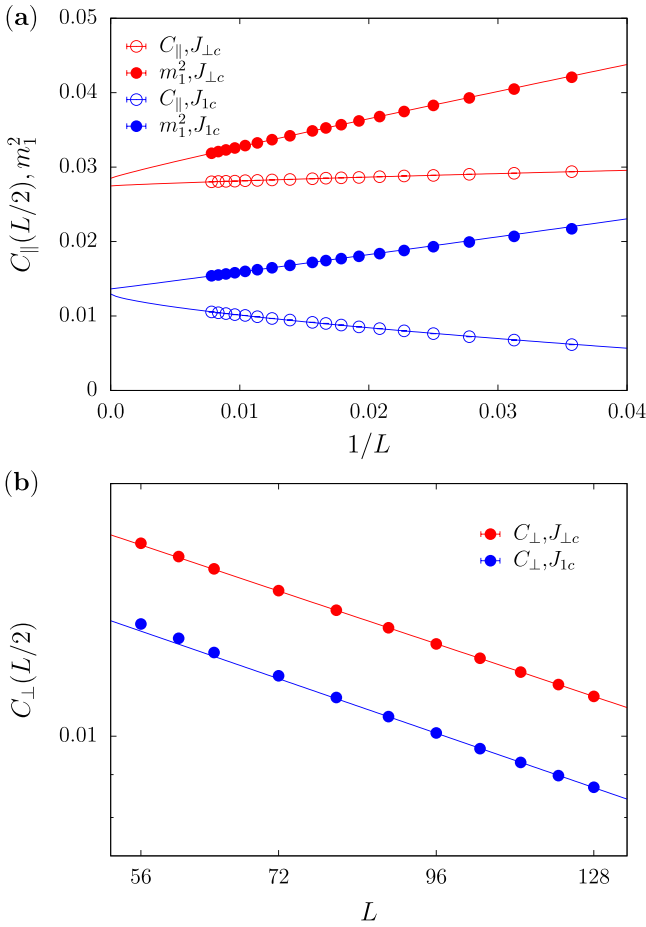


FIG. 6. (a) Squared surface ferromagnetic magnetization m_1^2 and the correlations $C_{\parallel}(L/2)$ versus $1/L$ and (b) the correlations $C_{\perp}(L/2)$ versus system size L on a log-log scale at two bulk critical points. The lines are fits according to Eqs. (16)–(18).

In this paper, we have shown that the QCPs between the striped phase and the two SPT phases (the UH and DHFM phases) belong to the 3D O(3) UC. Both of them have gapless edge modes on the surfaces formed by the ends of the ladders, which are not dangling. In the next two subsections, we will check the various SCBs listed above on these surfaces and show that the gapless edge modes lead to unexpected extraordinary SCBs, which suggests that the two SPT states, i.e., DHFM and UH, are topologically different from the SPT state (DHAF) studied in Ref. [20] and the SPT state of the AFM-coupled spin-1 chain [19].

A. Surface critical behaviors at the QCP between the UH and striped phases

We first study the SCBs associated with the bulk critical point ($J_{\perp} = -1, J_{1c}$) separating the striped magnetic ordered phase from the SPT UH phase.

The numerical results of $C_{\parallel}(L/2)$ and $m_1^2(L)$ as functions of size L are graphed in Fig. 6(a) and $C_{\perp}(L/2)$ as a function of L are plotted in Fig. 6(b).

Evidently, the extraordinary-log SCBs are excluded since $C_{\parallel}(L/2)$ increases with size L . We then try to analyze $C_{\parallel}(L/2)$ according to Eq. (16).

TABLE II. Finite-size scaling analysis of $C_{\parallel}(L/2)$, $m_1^2(L)$, and $C_{\perp}(L/2)$ at bulk critical point J_{1c} to obtain surface critical exponents η_{\parallel} , y_{h1} , and η_{\perp} . Correction term L^{-1} included in the fitting formula Eqs. (16)–(18) are denoted by yes, not included are denoted by no. Reduced χ^2 (R- χ^2) and p value of χ^2 (P- χ^2) are also listed.

	L_{\min}	η_{\parallel}	R/P- χ^2
Yes	56	-0.33(5)	0.98/0.45
	64	-0.34(8)	1.15/0.32
	72	-0.3(1)	1.38/0.22
No	72	-0.29(1)	1.18/0.30
	88	-0.30(2)	0.76/0.55
	96	-0.30(3)	1.0/0.39
	L_{\min}	y_{h1}	R/P- χ^2
Yes	48	1.69(8)	1.34/0.20
	56	1.7(1)	1.08/0.37
	64	1.7(2)	0.42/0.86
No	88	1.641(4)	1.71/0.14
	96	1.64(1)	1.50/0.21
	104	1.65(1)	0.53/0.59
	L_{\min}	η_{\perp}	R/P- χ^2
Yes	80	-0.56(4)	0.55/0.70
	88	-0.55(6)	0.61/0.61
	96	-0.6(2)	0.49/0.61
No	80	-0.48(1)	1.88/0.09
	88	-0.48(1)	0.83/0.51
	96	-0.48(1)	1.00/0.39

Supposing $\eta_{\parallel} < 0$, we can ignore the L^{-1} term for large L . Alternatively, if $\eta_{\parallel} > 0$, the second term in Eq. (16) can be ignored for large L . In either case, as $C_{\parallel}(L/2)$ increases with size L , it is evident that $C_{\parallel} > 0$. Fitting Eq. (16) with η_{\parallel} , C_{\parallel} , and a_1 free, ignoring the L^{-1} term, results in $C_{\parallel} = 0.0124(6)$. However, η_{\parallel} is near 0, making it difficult to separate the singular parts from the analytic term $1/L$. We have also tried to include the $1/L$ term in Eq. (16) in the fitting; however, this does not lead to a meaningful estimate of η_{\parallel} .

We fit $m_1^2(L)$ according to Eq. (18) with y_{h1} , m_1^2 , and c_1 free, ignoring analytic terms, resulting in $m_1^2 = 0.013(1)$, in good agreement with C_{\parallel} within the error bars, thus supporting long-range order on the surface. Unfortunately, in this fitting, we find y_{h1} nearly 1.5; again, it is difficult to separate the singular parts from the analytical correction $1/L$.

With the long-range order on the surface determined, it is tempting to fix $C_{\parallel} = m_1^2 = 0.0127$ in the fitting formula Eq. (16) for $C_{\parallel}(L)$ and Eq. (18) for $m_1^2(L)$, and fit for η_{\parallel} and y_{h1} again. By gradually excluding small sizes, we achieve stable fits for both $C_{\parallel}(L)$ and $m_1^2(L)$, with the analytic correction $1/L$ term included and not included. The details of the fitting procedure are presented in Table II. Our final estimate of the exponent η_{\parallel} is $\eta_{\parallel} = -0.30(3)$ and the exponent y_{h1} is $y_{h1} = 1.65(1)$. The two exponents obey the scaling relation Eq. (20). However, these results are based on assuming values of C_{\parallel} and m_1^2 ; one should be cautious about the reliability of these estimates.

The finite-size scaling form in Eq. (17) is used to fit the data of $C_{\perp}(L/2)$. Stable fits are obtained for sufficiently large

sizes and are also listed in Table II. Our final estimate of the exponent η_{\perp} is $\eta_{\perp} = -0.48(1)$. The result is consistent with $\eta_{\perp} = -0.5050(10)$ found in the extraordinary transition on the dangling ladder surface of the 2D staggered Heisenberg model [21].

However, the exponents $\eta_{\parallel} = -0.30(3)$ and $\eta_{\perp} = -0.48(1)$ violate the relation in Eq. (19). Hence the value of $\eta_{\parallel} = -0.30(3)$, as well as $y_{h1} = 1.65(1)$, become more doubtful.

B. Surface critical behaviors at the QCP between the DHFM and the striped phases

We then check the SCBs at the critical point ($J_{\perp c}, J_{\parallel} = 1$) where the SPT DHFM phase transfers to the striped magnetic ordered phase.

The numerical results of $C_{\parallel}(L/2)$ and m_1^2 versus L are plotted in Fig. 6(a).

The SPT DHFM state is the ground state of weakly FM-CDLs. The diagonal ladder, similar to the usual ladder with FM rungs, behaves like a spin-1 chain, and its VB ground state is also odd [25]. As discussed in the Introduction, both the DHFM state and the UH state can be regarded as FM-coupled spin-1 chains. Therefore, we expect qualitatively the same SCBs as those at the UH and the striped phase QCP and exclude the extraordinary-log scenario. Nevertheless, we have checked the extraordinary-log behaviors. Fitting $C_{\parallel}(L/2)$ according to Eq. (21) yields $q = 0.09(20)$, and similar fitting to $m_1^2(L)$ yields $q = 0.156(7)$. Hence, although we cannot completely exclude the extraordinary-log SCB, we conclude that such behavior is unlikely.

Fitting these data according to Eqs. (16) and (18) with the same procedure as at critical point ($J_{\perp} = -1, J_{\parallel c}$), we obtain $C_{\parallel} = 0.0275(3)$ and $m_1^2 = 0.028(2)$, which are consistent within error bars. This indicates the existence of a long-range order on the surface. Again, η_{\parallel} is found near 0 and $y_{h1} \approx 1.5$. It is difficult to separate the singular parts from the analytic correction.

We then fix $C_{\parallel} = m_1^2 = 0.0275$ in the fitting of Eqs. (16) and (18) to $C_{\parallel}(L/2)$ and $m_1^2(L)$, respectively. We achieve a stable fit with the $1/L$ term included or not included in the fitting procedure for sufficiently large L_{\min} . The results are listed in Table III. Our final estimates of the exponents are $\eta_{\parallel} = -0.22(7)$ and $y_{h1} = 1.64(1)$. The two exponents satisfy the scaling relation Eq. (20) and are consistent with the results at ($J_{\perp} = -1, J_{\parallel c}$). Again, we have reservations about the values of these exponents.

The numerical results of $C_{\perp}(L/2)$ as functions of L are plotted in Fig. 6(b). Stable fits are obtained by gradually excluding data of sizes smaller than L_{\min} . The procedure is presented in Table III. Our final estimate is $\eta_{\perp} = -0.498(2)$. The exponent is consistent with the results at $J_{\parallel c}$ as well as the $\eta_{\perp} = -0.5050(10)$ found in the extraordinary transition on a special surface of the 2D staggered Heisenberg model [21].

Apparently, η_{\parallel} and η_{\perp} also challenge the relation in Eq. (19). This fact makes the value of $\eta_{\parallel} = -0.22(7)$, as well as $y_{h1} = 1.64(1)$, suspect; however, they agree with the corresponding exponents found at the critical point ($J_{\perp} = -1, J_{\parallel c}$).

It is instructive to compare the above SCBs to those on the same surface at the critical point $J_{\perp 1c}$ between the DHAF phase and the AFM phase, see Fig. 2, which has been studied

TABLE III. Finite-size scaling analysis of $C_{\parallel}(L/2)$, $m_1^2(L)$, and $C_{\perp}(L/2)$ at bulk critical point $J_{\perp c}$ to obtain surface critical exponents η_{\parallel} , y_{h1} , and η_{\perp} , respectively. Fits with correction terms L^{-1} included are denoted by yes, those without L^{-1} term are denoted by no. Reduced χ^2 (R- χ^2) and p value of χ^2 (P- χ^2) are also listed.

	L_{\min}	η_{\parallel}	R/P- χ^2
Yes	44	-0.26(13)	0.34/0.97
	48	-0.28(16)	0.37/0.96
	56	-0.5(4)	0.26/0.97
No	72	-0.20(4)	0.23/0.96
	80	-0.19(5)	0.27/0.93
	88	-0.22(7)	0.27/0.90
	L_{\min}	y_{h1}	R/P- χ^2
Yes	72	1.70(5)	0.32/0.89
	80	1.71(6)	0.39/0.81
	88	1.7(1)	0.52/0.66
No	72	1.63(1)	1.66/0.12
	80	1.63(1)	1.03/0.39
	96	1.64(1)	0.70/0.55
	L_{\min}	η_{\perp}	R/P- χ^2
Yes	80	-0.52(2)	0.25/0.91
	88	-0.52(3)	0.34/0.80
	96	-0.53(4)	0.45/0.64
No	80	-0.497(1)	0.86/0.51
	88	-0.498(2)	0.52/0.72
	96	-0.499(2)	0.52/0.67

in our recent paper [20]. We found the parallel spin correlation decays to zero in power law, $C_{\parallel}(L/2) \sim L^{-(d+z-2+\eta_{\parallel})}$, with $\eta_{\parallel} = -0.511(2)$, indicating that there is *no* surface order. The scaling behavior of the surface staggered magnetic susceptibility $\chi_{s1}(L)$ also suggests that the SCB is not extraordinary, but nonordinary with exponent $y_{h1} = 1.756(3)$. Furthermore, in the Appendix, we present direct calculation of the surface staggered magnetization m_{s1}^2 . The results show that the surface staggered magnetization disappears at the thermodynamic limit, which further supports the conclusion that the SCBs at $J_{\perp 1c}$ are different from those at the QCP $J_{\parallel c}$ and $J_{\perp c}$.

V. DISCUSSION AND CONCLUSION

Using QMC simulations, we have studied the spin-1/2 Heisenberg model on the 2D CDL lattice with tunable ferromagnetic interladder couplings. The model can also be considered the spin-1/2 Heisenberg model on the 2D coupled FM usual ladders with tunable AFM diagonal couplings. We have studied the phases and phase transitions when the interladder coupling is tuned. We have shown that the model realizes two 2D SPT Haldane phases, the UH and the DHFM phases, when the two kinds of ladders are weakly coupled and that the model enters the striped magnetic ordered phase when the couplings of the ladders are strong enough. We have demonstrated that the two QCPs separating the SPT phases and the striped phase are in the 3D O(3) UC; the topological properties of the SPT phases do not affect the universal properties of the bulk phase transitions.

We have also studied the surface states of the two SPT phases and found gapless surface modes on the surfaces formed by the ends of the ladders. Unlike the surface configurations of the coupled Haldane chains [19] and that of the spin-1/2 CDL model with ladder coupling $J_{\perp} > 0$ [20] in the corresponding SPT Haldane phases, where the spin-1/2 excitations at the ends of the chains/ladders are coupled antiferromagnetically, here the spin-1/2 excitations at the ends of the ladders are coupled ferromagnetically. However, these surface excitations should not be viewed as a 1D ferromagnetic $S = 1/2$ chain, which is ordered. Instead, the gapless surface modes in both SPT phases should be considered to originate purely from the bulk-edge correspondence of the topologically ordered bulk state.

We have focused on the SCBs at the two bulk critical points. Unlike in the CHC model and the AFM-coupled spin-1/2 CDL model, where the gapless edge modes of the SPT phases induce nonordinary SCBs, we showed that the gapless surface states of the UH and the DHFM SPT states of the current model lead to extraordinary SCBs at the two bulk QCPs with magnetically ordered surfaces. These results show that the SPT state of the FM-coupled CDLs model and the SPT state of the diagonally AFM-coupled FM usual ladders are topologically different from the SPT state of the AFM-coupled CDLs model according to the bulk-edge correspondence of a topologically ordered state.

Finally, we would like to mention that an SPT state leading to extraordinary SCB at a QCP is a surprise. To our knowledge, there is no theoretical explanation for this. Therefore, further investigations are called for.

ACKNOWLEDGMENTS

We thank Prof. H. Q. Lin and Dr. Wenjing Zhu for their valuable discussions. This work was supported by the National Natural Science Foundation of China under Grants No. 12175015 and No. 11734002. The authors acknowledge the support the Super Computing Center of Beijing Normal University extended.

APPENDIX: STAGGERED SURFACE MAGNETIZATION AT CRITICAL POINT $J_{\perp c}$ BETWEEN THE DHAF AND THE AFM PHASES

The staggered surface magnetization $m_{s1}(L)$ is defined as follows:

$$m_{s1}(L) = \frac{1}{L} \sum_{i \in \text{surface}} \phi_i S_i^z, \quad (\text{A1})$$

where the summation is restricted on the surface, $\phi_i = \pm 1$ depending on the sublattice to which i belongs.

Figure 7 shows the squared staggered surface magnetization $m_{s1}^2(L)$ on the surface formed by the ends of coupled

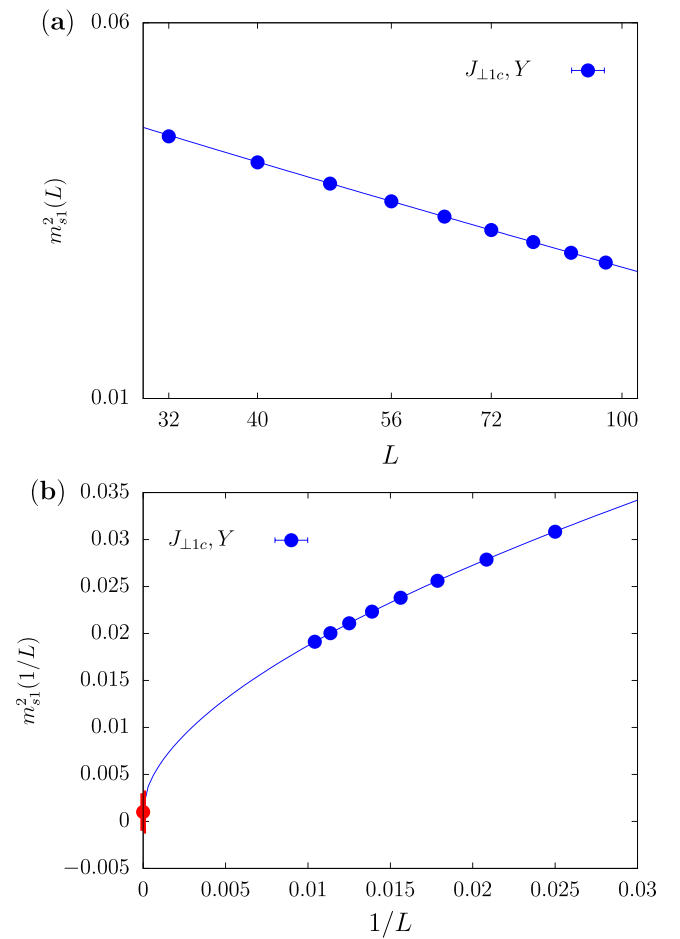


FIG. 7. Squared staggered surface magnetization $m_{s1}^2(L)$ versus (a) linear size L on a log-log scale and (b) $1/L$ at the bulk critical point $J_{\perp c}$. The red symbol shows the extrapolated value at the thermodynamic limit, which is zero within the error bar.

ladders referred to as the Y surface in Ref. [20] at the bulk critical point $J_{\perp c}$.

We fit the data of the $m_{s1}^2(L)$ according to

$$m_{s1}^2(L) = m_{s1}^2 + c_1 L^{-2(d+z-1-y_{h1})}, \quad (\text{A2})$$

with m_{s1}^2 set to zero and obtain a statistically sound fit with $y_{h1} = 1.74(1)$, which is coincident with $y_{h1} = 1.756(3)$ obtained from the scaling behavior of the staggered magnetic susceptibility χ_{s1} in our previous paper [20], as shown in Fig. 7(a).

We have also tried to fit the data of $m_{s1}^2(L)$ according to Eq. (A2) with m_{s1}^2 free. We find $m_{s1}^2 = 0.001(2)$, which is zero within the error bar, as illustrated in Fig. 7(b).

The finite and disappearing magnetization on the surface indicates that the DHAF phase and DHFM, UH phase are topologically different according to bulk-edge correspondence.

[1] L. Landau and E. Lifshitz, *Statistical Physics*, Vol. 5 (Elsevier Butterworth-Heinemann, Burlington, MA, 1980).

[2] K. G. Wilson and J. Kogut, The renormalization group and the ϵ expansion, *Phys. Rep.* **12**, 75 (1974).

- [3] J. Cardy, in *Scaling and Renormalization in Statistical Physics*, Cambridge Lecture Notes in Physics Vol. 5 (Cambridge University Press, Cambridge, 1996), p. 238.
- [4] K. Binder and P. C. Hohenberg, Surface effects on magnetic phase transitions, *Phys. Rev. B* **9**, 2194 (1974).
- [5] K. Binder, in *Phase Transitions and Critical Phenomena*, edited by C. Domb and J. L. Lebowitz (Academic Press, London, 1983), Vol. 8.
- [6] Y. Deng, H. W. J. Blöte, and M. P. Nightingale, Surface and bulk transitions in three-dimensional $O(n)$ models, *Phys. Rev. E* **72**, 016128 (2005).
- [7] M. A. Metlitski, Boundary criticality of the $O(N)$ model in $d = 3$ critically revisited, *SciPost Phys.* **12**, 131 (2022).
- [8] F. Parisen Toldin, Boundary Critical Behavior of the Three-Dimensional Heisenberg Universality Class, *Phys. Rev. Lett.* **126**, 135701 (2021).
- [9] M. Hu, Y. Deng, and J.-P. Lv, Extraordinary-Log Surface Phase Transition in the Three-Dimensional XY Model, *Phys. Rev. Lett.* **127**, 120603 (2021).
- [10] F. Parisen Toldin and M. A. Metlitski, Boundary Criticality of the 3D $O(N)$ Model: From Normal to Extraordinary, *Phys. Rev. Lett.* **128**, 215701 (2022).
- [11] J. Padayasi, A. Krishnan, M. A. Metlitski, I. A. Gruzberg, and M. Meineri, The extraordinary boundary transition in the 3D $O(N)$ model via conformal bootstrap, *SciPost Phys.* **12**, 190 (2022).
- [12] X. Zou, S. Liu, and W. Guo, Surface critical properties of the three-dimensional clock model, *Phys. Rev. B* **106**, 064420 (2022).
- [13] Z.-C. Gu and X.-G. Wen, Tensor-entanglement-filtering renormalization approach and symmetry-protected topological order, *Phys. Rev. B* **80**, 155131 (2009).
- [14] F. Pollmann, A. M. Turner, E. Berg, and M. Oshikawa, Entanglement spectrum of a topological phase in one dimension, *Phys. Rev. B* **81**, 064439 (2010).
- [15] X. Chen, Z.-C. Gu, Z.-X. Liu, and X.-G. Wen, Symmetry-protected topological orders in interacting bosonic systems, *Science* **338**, 1604 (2012).
- [16] F. D. M. Haldane, Nonlinear field theory of large-spin Heisenberg antiferromagnets: Semiclassically Quantized Solitons of the One-Dimensional Easy-Axis Néel State, *Phys. Rev. Lett.* **50**, 1153 (1983).
- [17] I. Affleck, T. Kennedy, E. H. Lieb, and H. Tasaki, Rigorous Results on Valence-Bond Ground States in Antiferromagnets, *Phys. Rev. Lett.* **59**, 799 (1987).
- [18] L. Zhang and F. Wang, Unconventional Surface Critical Behavior Induced by a Quantum Phase Transition from the Two-Dimensional Affleck-Kennedy-Lieb-Tasaki Phase to a Néel-Ordered Phase, *Phys. Rev. Lett.* **118**, 087201 (2017).
- [19] W. Zhu, C. Ding, L. Zhang, and W. Guo, Surface critical behavior of coupled Haldane chains, *Phys. Rev. B* **103**, 024412 (2021).
- [20] Z. Wang, F. Zhang, and W. Guo, Bulk and surface critical behavior of a quantum Heisenberg antiferromagnet on two-dimensional coupled diagonal ladders, *Phys. Rev. B* **106**, 134407 (2022).
- [21] C. Ding, L. Zhang, and W. Guo, Engineering Surface Critical Behavior of $(2 + 1)$ -Dimensional $O(3)$ Quantum Critical Points, *Phys. Rev. Lett.* **120**, 235701 (2018).
- [22] L. Weber, F. Parisen Toldin, and S. Wessel, Nonordinary edge criticality of two-dimensional quantum critical magnets, *Phys. Rev. B* **98**, 140403(R) (2018).
- [23] C. Ding, W. Zhu, W. Guo, and L. Zhang, Special transition and extraordinary phase on the surface of a $(2+1)$ -dimensional quantum Heisenberg antiferromagnet [SciPost Phys. (to be published)], [arXiv:2110.04762](https://arxiv.org/abs/2110.04762).
- [24] E. Lieb, T. Schultz, and D. Mattis, Two soluble models of an antiferromagnetic chain, *Ann. Phys.* **16**, 407 (1961).
- [25] E. H. Kim, G. Fáth, J. Sólyom, and D. J. Scalapino, Phase transitions between topologically distinct gapped phases in isotropic spin ladders, *Phys. Rev. B* **62**, 14965 (2000).
- [26] W. J. L. Buyers, R. M. Morra, R. L. Armstrong, M. J. Hogan, P. Gerlach, and K. Hirakawa, Experimental Evidence for the Haldane Gap in a Spin-1 Nearly Isotropic, Antiferromagnetic Chain, *Phys. Rev. Lett.* **56**, 371 (1986).
- [27] E. Dagotto, Experiments on ladders reveal a complex interplay between a spin-gapped normal state and superconductivity, *Rep. Prog. Phys.* **62**, 1525 (1999).
- [28] K. Wierschem and P. Sengupta, Quenching the Haldane Gap in Spin-1 Heisenberg Antiferromagnets, *Phys. Rev. Lett.* **112**, 247203 (2014).
- [29] A. W. Sandvik and J. Kurkijärvi, Quantum Monte Carlo simulation method for spin systems, *Phys. Rev. B* **43**, 5950 (1991).
- [30] A. W. Sandvik, Stochastic series expansion method with operator-loop update, *Phys. Rev. B* **59**, R14157 (1999).
- [31] O. F. Syljuåsen and A. W. Sandvik, Quantum Monte Carlo with directed loops, *Phys. Rev. E* **66**, 046701 (2002).
- [32] K. Binder, Critical Properties from Monte Carlo Coarse Graining and Renormalization, *Phys. Rev. Lett.* **47**, 693 (1981).
- [33] K. Binder and D. P. Landau, Finite-size scaling at first-order phase transitions, *Phys. Rev. B* **30**, 1477 (1984).
- [34] E. L. Pollock and D. M. Ceperley, Path-integral computation of superfluid densities, *Phys. Rev. B* **36**, 8343 (1987).
- [35] A. W. Sandvik, Computational studies of quantum spin systems, *AIP Conf. Proc.* **1297**, 135 (2010).
- [36] M. P. A. Fisher, P. B. Weichman, G. Grinstein, and D. S. Fisher, Boson localization and the superfluid-insulator transition, *Phys. Rev. B* **40**, 546 (1989).
- [37] H. Shao, W. Guo, and A. W. Sandvik, Quantum criticality with two length scales, *Science* **352**, 213 (2016).
- [38] R. Guida and J. Zinn-Justin, Critical exponents of the N -vector model, *J. Phys. A: Math. Gen.* **31**, 8103 (1998).
- [39] M. Hasenbusch and E. Vicari, Anisotropic perturbations in three-dimensional $O(n)$ -symmetric vector models, *Phys. Rev. B* **84**, 125136 (2011).
- [40] M. Matsumoto, C. Yasuda, S. Todo, and H. Takayama, Ground-state phase diagram of quantum Heisenberg antiferromagnets on the anisotropic dimerized square lattice, *Phys. Rev. B* **65**, 014407 (2001).
- [41] I. Affleck and F. D. M. Haldane, Critical theory of quantum spin chains, *Phys. Rev. B* **36**, 5291 (1987).
- [42] M. den Nijs and K. Rommelse, Preroughening transitions in crystal surfaces and valence-bond phases in quantum spin chains, *Phys. Rev. B* **40**, 4709 (1989).
- [43] F. Anfuso and A. Rosch, Fragility of string orders, *Phys. Rev. B* **76**, 085124 (2007).
- [44] X.-G. Wen, Colloquium: Zoo of quantum-topological phases of matter, *Rev. Mod. Phys.* **89**, 041004 (2017).

- [45] H. W. Diehl, in *Phase Transitions and Critical Phenomena*, edited by C. Domb and J. L. Lebowitz (Academic Press, London, 1986), Vol. 10, pp. 75–267.
- [46] C.-M. Jian, Y. Xu, X.-C. Wu, and C. Xu, Continuous Néel-VBS quantum phase transition in non-local one-dimensional systems with $SO(3)$ symmetry, *SciPost Phys.* **10**, 033 (2021).
- [47] W. Zhu, C. Ding, L. Zhang, and W. Guo, Exotic surface behaviors induced by geometrical settings of the two-dimensional dimerized quantum XXZ model, [arXiv:2111.12336](https://arxiv.org/abs/2111.12336).